



HAL
open science

Layer-specific alterations to CA1 dendritic spines in a mouse model of Alzheimer's disease

S. Knafo

► **To cite this version:**

S. Knafo. Layer-specific alterations to CA1 dendritic spines in a mouse model of Alzheimer's disease. Hippocampus, 2010, 21 (10), pp.1037. 10.1002/hipo.20861 . hal-00686076

HAL Id: hal-00686076

<https://hal.science/hal-00686076>

Submitted on 7 Apr 2012

HAL is a multi-disciplinary open access archive for the deposit and dissemination of scientific research documents, whether they are published or not. The documents may come from teaching and research institutions in France or abroad, or from public or private research centers.

L'archive ouverte pluridisciplinaire **HAL**, est destinée au dépôt et à la diffusion de documents scientifiques de niveau recherche, publiés ou non, émanant des établissements d'enseignement et de recherche français ou étrangers, des laboratoires publics ou privés.

Layer-Specific Alterations to CA1 Dendritic Spines in a Mouse Model of Alzheimer's Disease

P. Merino-Serrais^{1*}, S. Knafo^{1,2*}, L. Alonso-Nanclares¹, I. Fernaud-Espinosa¹ and J. DeFelipe¹

1. Instituto Cajal (CSIC), Madrid, Spain & Laboratorio de Circuitos Corticales, Centro de de Tecnología Biomédica, Universidad Politécnica de Madrid, Madrid, Spain.
2. Centro de Biología Molecular “Severo Ochoa”, Consejo Superior de Investigaciones Científicas (CSIC) - Universidad Autónoma de Madrid, Madrid, Spain.

Corresponding author: Dr S. Knafo, Centro de Biología Molecular “Severo Ochoa”, Consejo Superior de Investigaciones Científicas (CSIC) - Universidad Autónoma de Madrid, Madrid, Spain. email: sknafo@cbm.uam.es

Abbreviations: AD, Alzheimer's Disease, A β , Amyloid β , APP, amyloid precursor protein.

* These authors contributed equally to this work

ABSTRACT: Why memory is a particular target for the pathological changes in Alzheimer's Disease (AD) has long been a fundamental question when considering the mechanisms underlying this disease. It has been established from numerous biochemical and morphological studies that AD is, at least initially, a consequence of synaptic malfunction provoked by Amyloid β ($A\beta$) peptide. APP/PS1 transgenic mice accumulate $A\beta$ throughout the brain, and they have therefore been employed to investigate the effects of $A\beta$ overproduction on brain circuitry and cognition. Previous studies show that $A\beta$ overproduction affects spine morphology in the hippocampus and amygdala, both within and outside plaques (Knafo et al., 2009a;Knafo et al., 2009b). Hence, we conducted a detailed analysis of dendritic spines located in the stratum oriens and stratum radiatum of the CA1 hippocampal subfield of APP/PS1 mice. Three-dimensional analysis of 18,313 individual dendritic spines revealed a substantial layer-specific decrease in spine neck length and an increase in the frequency of spines with a small head volume. Since dendritic spines bear most of the excitatory synapses in the brain, changes in spine morphology may be one of the factors contributing to the cognitive impairments observed in this AD model.

The presence of $A\beta$ plaques is one of the pathological hallmarks of AD, and they have been associated with changes in neurite morphology and dendritic spine density (Tsai et al., 2004;Spires et al., 2005;Knafo et al., 2009a;Knafo et al., 2009b). Apart from amyloid plaques, the $A\beta$ peptide accumulates in different forms in AD: intracellular $A\beta$ and oligomeric $A\beta$. Indeed, it has been demonstrated that spine heads are targets of oligomeric $A\beta$ (Lacor *et al.* 2007), and it has been suggested that targeting and functional disruption of particular synapses by $A\beta$ oligomers may provide a molecular basis for the specific memory loss in AD (Lacor et al., 2007). Nevertheless, previous studies indicate that there is only a weak correlation between plaque load and cognitive functions (Terry et al., 1991). In fact, plaques are sometimes detected even in non-demented patients (Price et al., 2009) and cognitive decline is better reflected by the level of soluble $A\beta$ oligomers, distributed diffusely outside the plaques (Selkoe, 2002). Moreover, at least in aged mice bearing AD mutations, plaques occupy a negligible fraction of the neuropil,

less than 5% (Cohen et al., 2009;Knafo et al., 2009a;Knafo et al., 2009b), and therefore, it is unlikely that cognitive impairment in these mice arises solely from changes in synapses within the plaques. Hence, AD neuropathological research is increasingly focusing on the changes in plaque-free regions of the neuropil and in AD-like pathology prior to plaque appearance. Here we have analyzed dendritic spines in the CA1 subfield, an area critical for spatial orientation and learning (Andersen et al., 2006), in order to determine the microstructural basis of the hippocampal-dependent cognitive impairment in APP/PS1 mice (Malm et al., 2007). Dendritic spines represent the major postsynaptic elements of excitatory synapses in the cerebral cortex (Gray, 1959) and they are fundamental to memory, learning and cognition (Lamprecht and LeDoux, 2004). Dendritic spines undergo remarkable activity-dependent structural changes (Lang et al., 2004;Tsai et al., 2004) and they are targets of oligomeric A β (Lacor et al., 2007). Therefore, spine morphology may be associated with A β pathology and synaptic malfunction. We show that in APP/PS1 mice, CA1 spines necks are significantly shorter in the stratum oriens. In addition, the frequency of spines with a small head augments in the same subfield of the *stratum radiatum*. These findings indicate that circuits in the *stratum radiatum* and the *stratum oriens* might be affected differently by AD-related mutations. In addition, this study suggests that dendritic spine morphology reflects the synaptic malfunction arising from A β overexpression.

We used a transgenic mouse line (12-14 month old male mice) expressing a Mo/Hu APP695swe construct in conjunction with the exon 9 deleted variant of human presenilin 1 (PS1-dE9: (Scheuner et al., 1996). Age-matched littermates served as controls (Tg-). The mice were perfused with 4% paraformaldehyde and coronal sections of the fixed brain were obtained. A total of 270 pyramidal neurons from Tg⁻ mice and 262 neurons from APP/PS1 mice were microinjected individually with Alexa594 (Invitrogen, Eugene, OR, Fig. 1 a, b), and plaques were counterstained with thioflavin-s after injection (Fig. 1 a-c). The plaques and dendrites in the stratum oriens (corresponding to basal dendrites) and in the stratum radiatum (collateral apical dendrites) were scanned with a Leica laser scanning multispectral confocal microscope (TCS SP5) using 488 and 594 nm laser lines. Image stacks (Physical size 76.9 \times 76.9 μ m,

logical size 1024×1024 pixels) consisted of 100-350 image planes. A 63 \times Glycerol-immersion lens (NA, 1.3; working distance, 280 μm ; refraction index, 1.45) was used with a calculated optimal zoom factor of 3.2 and a z-step of 0.14 μm (voxel size, $75.1 \times 75.1 \times 136.4$ nm). These settings and optics represent the highest resolution currently possible with confocal microscopy. After acquisition, the stacks were processed over ten iterations with a three-dimensional blind deconvolution algorithm (Autodeblur; Autoquant, Media Cybernetics) to reduce the out-of-focus light, and thereby removing the haze and the blur, restoring vital details to the datasets (supplemental figure 1 b). The stacks were then opened with Imaris 6.0 (Bitplane AG, Zurich, Switzerland), a three-dimensional image processing software. In stacks containing images of A β plaques (green), the green channel was deleted and the stacks were coded (the codes were not broken until the quantitative analysis had been completed). Spine density measurements and their morphology were assessed by another investigator using only the red channel to assure impartiality (Fig. 1 f, i). For spine density measurements, image stacks were viewed with a computerized data collection system (NeuroLucida 7.1 Confocal module; MicroBrightfield, Inc., Williston, VT, USA), the image of the acquired dendrites was traced in three-dimensions and the spines were marked during tracing. To assess the morphology of spines, a solid surface that exactly matched the contours of the head was constructed for each spine using Imaris (Fig. 1 i), and the length of the spine neck was measured manually in three-dimensions using the same software (Isosurface module, see detailed methods). To estimate the density of plaques, plaques were immunostained with an anti-A β antibody in serial sections taken from the same mice, and unbiased stereology rules were applied using optical fractionation and the Nucleator probe (Moller et al., 1990). For all the morphological parameters measured, the values were averaged to give a neuron mean, and neurons from each animal were averaged for the animal mean. Normality was tested using the Kolmogorov-Smirnov test and a two-tailed unpaired t-test was used to test for the overall effect. When more than two groups were compared, a one-way ANOVA was used, followed by Tukey's Multiple Comparison *post-hoc* test. Data are presented as the mean \pm SEM.

We examined 1,475 amyloid plaques and 532 injected pyramidal neurons by confocal microscopy (Fig. 1 a). We encountered only 5 dendrites that passed within plaques in the stratum oriens (basal dendrites) and no such dendrites in the stratum radiatum (apical dendrites). Typical plaques that were positive for thioflavin-s consisted of a core surrounded by a diffuse less dense ring. The dendrites passing through the plaques were located in the diffuse peripheral ring, as described previously (Cruz et al., 1997;Knafo et al., 2009a;Knafo et al., 2009b). Dendrites were categorized according to their location with respect to the A β plaques, as: (1) dendrites from transgene-negative (control) mice (Tg-); (2) dendrites located in a plaque-free area (Plaque-free); (3) segments of dendrites within a plaque (Plaque).

Spines have a shorter neck in plaque-free regions of the stratum oriens of APP/PS1 mice

The spine density in the stratum oriens was significantly different among the three categories of dendrites ($P = 0.006$, one-way ANOVA, Fig. 1 d). Accordingly, the spine density was significantly lower within plaques than in other categories of dendrites (0.85 ± 0.17 spines/ μm , $N = 4$). However, spine density for Plaque-free dendrites (1.33 ± 0.054 , $N = 7$) did not differ significantly from that of control (Tg-) dendrites (1.348 ± 0.070 , $N = 6$). Moreover, a Sholl analysis of the spine density at different distances from the soma revealed that the spine density for Plaque-free dendrites was similar to that of control dendrites over their entire length (Fig. 1 e).

Spine neck length and head volume were measured in three dimensions in confocal image stacks. Due to the extensive loss of spines within plaques, the spines within plaques (31 spines) were not included in the analysis of head and neck dimensions. Significant differences in the average spine neck length were found between the two dendritic categories ($P = 0.018$, t-test, Fig. 1 g-h). Spines in the APP/PS1 mice had a significantly shorter neck (26%) than spines in Tg- mice spines (0.548 ± 0.040). Head volume was not significantly different among the two categories of dendrites ($P = 0.88$, t-test, Fig. j-k), and was $0.056 \pm 0.003 \mu\text{m}^3$, for Tg- dendrites ($N=6$, 5,709 spines) and $0.055 \pm 0.003 \mu\text{m}^3$ for plaque-free dendrites ($N = 7$, 5,145 spines). Thus, in the

stratum oriens of APP/PS1 mice, spine density is decreased within plaques and spines are shorter outside plaques.

Small-headed spines are more frequent in plaque-free regions of the stratum radiatum of APP/PS1 mice

Spine density and morphology were examined in apical branches protruding from the main apical trunk. These dendrites were located up to 300 μm from the *stratum pyramidale* (cell body layer). Dendrites located in the *stratum lacunosum-moleculare* were not included in the analysis. The average spine density along the apical dendrites in the *stratum radiatum* did not differ significantly in APP/PS1 mice when compared to the control mice (1.71 ± 0.08 for Tg- mice and 1.83 ± 0.08 for APP/PS1 mice: $P = 0.62$, student t-test; Fig. 2 a-b). A Sholl analysis revealed that the density of spines on Plaque-free dendrites was not significantly different to that of control (Tg-) dendrites over their entire length (Fig. 2 c). By contrast to the *stratum oriens*, the neck length was similar in both groups ($P = 0.43$, t-test, Fig. 2 d,e), as it was $0.519 \pm 0.017 \mu\text{m}$ for Tg- dendrites and $0.494 \pm 0.024 \mu\text{m}$ in APP/PS1 mice. The average head volume in this layer did not differ significantly between Tg- dendrites ($0.038 \pm 0.003 \mu\text{m}^3$: $N = 6$; 4,437 spines) and plaque-free regions ($0.033 \pm 0.003 \mu\text{m}^3$: $N = 7$; 6,044 spines. $P = 0.29$, t-test, Fig. 2 f). Nevertheless, the cumulative frequency curves clearly indicated a distinct distribution of head volumes in the smaller values (Fig. 2 g) and indeed, a significant increase (29%, $P = 0.01$, t-test) in the frequency of small-headed spines (head volume $< 0.03 \mu\text{m}^3$) was evident in the plaque-free areas of APP/PS1 mice (Fig. 2 h). Thus, we found an increase in the frequency of small-headed spines in the *stratum radiatum* of APP/PS1 mice.

Amyloid plaques occupy a small fraction of the CA1

We have described changes in dendritic spines within and outside of plaques that can affect local synaptic circuits. To quantitatively determine the impact of plaques on CA1 connectivity, we immunocytochemically stained A β plaques in serial sections of APP/PS1 brains (Supplemental Figure 2). Using unbiased stereology, we then determined the total number of plaques and their volume in the *stratum oriens* and *stratum radiatum*, from which we could calculate the total volume occupied by the plaques. The estimated

total number of CA1 plaques per mouse in one hemisphere was 1551 ± 272.6 (range 1045-2081 plaques/mouse, N=4; Table 1) in the *stratum oriens* and 1985 ± 183.8 (range 1533-2628 plaques/mouse, N=5) in the *stratum radiatum*. The density of plaques in the *stratum oriens* was 1138 ± 214.4 plaques/mm³, while it was 1174 ± 113.0 plaques/mm³ in the *stratum radiatum* (Table 1). The average plaque volume was 0.019 ± 0.002 mm³ in the *stratum oriens* and 0.029 ± 0.0029 mm³ in the *stratum radiatum* (P=0.04, t-test). The estimated volume occupied by A β plaques was 1.421 ± 0.201 % in the *stratum oriens* and 1.554 ± 0.195 % in the *stratum radiatum* (Table 1). These results suggest that under our experimental conditions, A β plaques occupy a relatively small fraction of the CA1 neuropil.

The current study shows that dendritic spines in the CA1 subfield are significantly affected by A β , both within plaques and in plaque-free regions. Importantly, some changes in spine morphology in this region were not evident in the dentate gyrus (Knafo et al., 2009a) or the amygdala (Knafo et al., 2009b) when studied with the same tools. For example, no significant differences were found in the length of spine neck in these regions, whereas the neck was significantly shorter in the *stratum oriens* of APP/PS1 mice. Moreover, spines in the *stratum oriens* are affected differently to spines in *stratum radiatum*, even within the CA1. These layer-specific morphological alterations are underscored by the fact that A β plaques occupy a similar total volume of both layers (Table 1), implying a similar A β load. Thus, we conclude that AD-related mutations have distinct effects on spines depending on their location. We also show here that dendrites within plaques are deficient in spines, in accordance with observations in other brain regions (Tsai et al., 2004;Knafo et al., 2009a;Knafo et al., 2009b). Spine loss within A β plaques can affect local synaptic circuits. However, since plaques occupy a minor fraction of the CA1 (below 2%), the morphological changes observed outside plaques are more likely to contribute to the synaptic and cognitive impairments found in APP/PS1 mice (Malm et al., 2007). We also found that spine density outside plaques is unchanged in APP/PS1 mice, in accordance to our previous studies into the dentate gyrus and amygdala (Knafo et al., 2009a;Knafo et al., 2009b). These findings imply that cognitive impairment in these mice (Malm et al., 2007) does not arise from changes in spine

density in plaque-free areas. Rather, it is likely that changes in spine morphology outside plaques contribute to these cognitive deficits.

The data presented here shows that the average spine neck length is shorter in the *stratum oriens* of APP/PS1 mice, both within and outside of the plaques. The morphology of the spine neck fulfils a key role in controlling the time window compartmentalization of calcium and other second messengers in spines (Yuste et al., 2000). The shortening of the spine neck in APP/PS1 mice may increase the diffusion between the spine and the dendrite. Spines with a fast diffusion equilibration along the spine neck may be unable to retain second messengers or activate proteins upon the LTP inducing stimulus (Bloodgood and Sabatini, 2005). This altered plasticity may eventually contribute to the cognitive impairment seen in APP/PS1 mice (Malm et al., 2007).

We also found that APP/PS1 mice have a higher proportion of spines with a small head volume in the *stratum radiatum*. Importantly, small spines are more abundant after processes of long-term depression (LTD), a form of synaptic plasticity significantly enhanced in many models of AD (Shankar et al., 2008). Spine head size determines the size and duration of synaptic Ca^{2+} transients (Majewska et al., 2000) and it is therefore correlated with the magnitude of signals transmitted to the dendritic shaft (Harris and Stevens, 1989; Murthy et al., 2000). Spines with smaller heads have smaller postsynaptic densities (Harris and Stevens, 1989) and contain less AMPA receptors on their heads when compared to spines with larger heads (Kharazia and Weinberg, 1999), resulting in less sensitivity to glutamate at these spines (Matsuzaki et al., 2001). It is therefore possible that the increase in the frequency of small-headed spines reflects long-term synaptic depression, thereby contributing to the cognitive impairment seen in this AD model. Moreover, it is possible that the greater frequency of spines with large heads in this layer reflects the loss of LTP in APP/PS1 mice (Trinchese et al., 2004). Therefore, the laminar specific changes observed in spine length might have an important functional consequence in certain hippocampal circuits. In summary, we show here that spines in the CA1 are morphologically modified, which may reflect the functional alterations at synapses induced by $A\beta$ overexpression in APP/PS1 mice.

ACKNOWLEDGEMENTS

We thank C. Hernández and B. García for assistance with the confocal microscopy, and Dr I. Ferrer (Institut Neuropatologia, Servei Anatomia Patològica, IDIBELL-Hospital Universitari de Bellvitge, Universitat de Barcelona, Hospitalet de Llobregat, Spain) for supplying the animals. This work was supported by grants from the following bodies: CIBERNED (CB06/05/0066), Fundació CIEN (Financiación de Proyectos de Investigación de Enfermedad de Alzheimer y enfermedades relacionadas 2008), the EU 6th Framework Program (PROMEMORIA LSHM-CT-2005-512012), the Spanish Ministerio de Educación Ciencia e Innovación (BFU2006-13395 and SAF2009-09394, and a research fellowship BES-2007-16542 to P. M-S.). S.K. is a Ramón y Cajal fellow from the Ministry of Science and Technology.

Reference List

- Andersen P, Morris RG, Amaral D, Bliss T, O'Keefe J. 2006. *The Hippocampus Book*. USA: Oxford University Press.
- Bloodgood BL, Sabatini BL. 2005. Neuronal activity regulates diffusion across the neck of dendritic spines. *Science* 310:866-869.
- Cohen E, Paulsson JF, Blinder P, Burstyn-Cohen T, Du D, Estepa G, Adame A, Pham HM, Holzenberger M, Kelly JW, Masliah E, Dillin A. 2009. Reduced IGF-1 signaling delays age-associated proteotoxicity in mice. *Cell* 139:1157-1169.
- Cruz L, Urbanc B, Buldyrev SV, Christie R, Gomez-Isla T, Havlin S, McNamara M, Stanley HE, Hyman BT. 1997. Aggregation and disaggregation of senile plaques in Alzheimer disease. *Proc Natl Acad Sci U S A* 94:7612-7616.
- Gray EG. 1959. Electron microscopy of synaptic contacts on dendrite spines of the cerebral cortex. *Nature* 183:1592-1593.
- Harris KM, Jensen FE, Tsao B. 1992. Three-dimensional structure of dendritic spines and synapses in rat hippocampus (CA1) at postnatal day 15 and adult ages: implications for the maturation of synaptic physiology and long-term potentiation [published erratum appears in *J Neurosci* 1992 Aug;12(8):following table of contents]. *J Neurosci* 12:2685-2705.
- Harris KM, Stevens JK. 1989. Dendritic spines of CA 1 pyramidal cells in the rat hippocampus: serial electron microscopy with reference to their biophysical characteristics. *J Neurosci* 9:2982-2997.
- Kharazia VN, Weinberg RJ. 1999. Immunogold localization of AMPA and NMDA receptors in somatic sensory cortex of albino rat. *J Comp Neurol* 412:292-302.
- Knafo S, Alonso-Nanclares L, Gonzalez-Soriano J, Merino-Serrais P, Feraud-Espinosa I, Ferrer I, Defelipe J. 2009a. Widespread Changes in Dendritic Spines in a Model of Alzheimer's Disease. *Cereb Cortex* 19:586-592.
- Knafo S, Venero C, Merino-Serrais P, Gonzalez-Soriano J, Feraud-Espinosa I, Ferrer I, Santpere G, Defelipe J. 2009b. Morphological alterations to neurons of the amygdala and impaired fear conditioning in a transgenic mouse model of Alzheimer's disease. *The journal of pathology* In Press.
- Lacor PN, Buniel MC, Furlow PW, Sanz Clemente A, Velasco PT, Wood M, Viola KL, Klein WL. 2007. A β Oligomer-Induced Aberrations in Synapse Composition, Shape, and Density Provide a Molecular Basis for Loss of Connectivity in Alzheimer's Disease. *J Neurosci* 27:796-807.
- Lamprecht R, LeDoux J. 2004. Structural plasticity and memory. *Nat Rev Neurosci* 5:45-54.

- Lang C, Barco A, Zablow L, Kandel ER, Siegelbaum SA, Zakharenko SS.2004. Transient expansion of synaptically connected dendritic spines upon induction of hippocampal long-term potentiation. *Proceedings of the National Academy of Sciences of the United States of America* 101:16665-16670.
- Majewska A, Tashiro A, Yuste R.2000. Regulation of Spine Calcium Dynamics by Rapid Spine Motility. *J Neurosci* 20:8262-8268.
- Malm TM, Iivonen H, Goldsteins G, Keksa-Goldsteine V, Ahtoniemi T, Kanninen K, Salminen A, Auriola S, Van Groen T, Tanila H, Koistinaho J.2007. Pyrrolidine Dithiocarbamate Activates Akt and Improves Spatial Learning in APP/PS1 Mice without Affecting β -Amyloid Burden. *J Neurosci* 27:3712-3721.
- Matsuzaki M, Ellis-Davies GC, Nemoto T, Miyashita Y, Iino M, Kasai H.2001. Dendritic spine geometry is critical for AMPA receptor expression in hippocampal CA1 pyramidal neurons
1. *Nat Neurosci* 4:1086-1092.
- Moller A, Strange P, Gundersen HJ.1990. Efficient estimation of cell volume and number using the nucleator and the disector. *J Microsc* 159:61-71.
- Murthy VN, Sejnowski TJ, Stevens CF.2000. Dynamics of dendritic calcium transients evoked by quantal release at excitatory hippocampal synapses. *Proc Natl Acad Sci U S A* 97:901-906.
- Paxinos G, Franklin KBJ. 2001. *The Mouse Brain in Stereotaxic Coordinates*, Deluxe Second Edition. San Diego, California: Academic Press.
- Price JL, et al.2009. Neuropathology of nondemented aging: presumptive evidence for preclinical Alzheimer disease. *Neurobiol Aging* 30:1026-1036.
- Scheuner D, et al.1996. Secreted amyloid beta-protein similar to that in the senile plaques of Alzheimer's disease is increased in vivo by the presenilin 1 and 2 and APP mutations linked to familial Alzheimer's disease. *Nat Med* 2:864-870.
- Selkoe DJ.2002. Alzheimer's disease is a synaptic failure. *Science* 298:789-791.
- Shankar GM, Li S, Mehta TH, Garcia-Munoz A, Shepardson NE, Smith I, Brett FM, Farrell MA, Rowan MJ, Lemere CA, Regan CM, Walsh DM, Sabatini BL, Selkoe DJ.2008. Amyloid- β protein dimers isolated directly from Alzheimer's brains impair synaptic plasticity and memory. *Nat Med* 14:837-842.
- Spires TL, Meyer-Luehmann M, Stern EA, McLean PJ, Skoch J, Nguyen PT, Bacskai BJ, Hyman BT.2005. Dendritic Spine Abnormalities in Amyloid Precursor Protein Transgenic Mice Demonstrated by Gene Transfer and Intravital Multiphoton Microscopy. *J Neurosci* 25:7278-7287.

Stark AK, Pelvig DP, Jorgensen AM, Andersen BB, Pakkenberg B.2005. Measuring morphological and cellular changes in Alzheimer's dementia: a review emphasizing stereology. *Curr Alzheimer Res* 2:449-481.

Terry RD, Masliah E, Salmon DP, Butters N, DeTeresa R, Hill R, Hansen LA, Katzman R.1991. Physical basis of cognitive alterations in Alzheimer's disease: synapse loss is the major correlate of cognitive impairment. *Ann Neurol* 30:572-580.

Trinchese F, Liu S, Battaglia F, Walter S, Mathews PM, Arancio O.2004. Progressive age-related development of Alzheimer-like pathology in APP/PS1 mice. *Ann Neurol* 55:801-814.

Trommald M, Hulleberg G.1997. Dimensions and density of dendritic spines from rat dentate granule cells based on reconstructions from serial electron micrographs. *J Comp Neurol* 377:15-28.

Tsai J, Grutzendler J, Duff K, Gan WB.2004. Fibrillar amyloid deposition leads to local synaptic abnormalities and breakage of neuronal branches. *Nat Neurosci* 7:1181-1183.

Yuste R, Majewska A, Holthoff K.2000. From form to function: calcium compartmentalization in dendritic spines. *Nat Neurosci* 3:653-659.

FIGURE LEGENDS

Fig. 1. Spines are shorter in the *stratum oriens* of APP/PS1 mice. **(a)** A panoramic view of neurons injected with Alexa 594 (red) and thioflavin-s positive plaques (green) in the hippocampus (20 \times , oil). **(b)** Representative projection images (40 \times , oil) of injected neurons and plaques in Tg- (*left*) and APP/PS1 mice (*right*). The plaques seen in the *stratum radiatum* (apical dendrites) are located close to labeled dendrites but they do not contain dendrites, as determined by 3-dimensional analysis. **(c)** An example of a dendrite located in the *stratum oriens* passing through a plaque and showing a decrease in spine density within the plaque. **(d)** Spine density is decreased significantly within the plaques. Note that the spine density is similar in Tg- mice and in the plaque-free areas of APP/PS1 mice. **(e)** The spine density as a function of the distance from the soma (Sholl Analysis) is similar in Tg- and APP/PS1 mice in plaque-free regions. Note the similarity in spine density along the length of the dendrite. **(f)** Representative projection images of dendrites from Tg- and APP/PS1 mice (63 \times , glycerol). Necks are marked as was done for measurements **(g)** Decreased average neck length for spines in APP/PS1 mice outside plaques. **(h)** Cumulative frequency plots showing the distribution of spine neck length, indicating a shift towards lower values in the entire spine population. **(i)** Representative images of dendritic segments with the contours of the spine heads constructed for each spine (see supplemental figure 1 for details). **(j-k)** The head volume is similar for Tg- and APP/PS1 mice. *, $P < 0.05$, Tukey's Multiple Comparison *post-hoc* test. Scale bar, **(a)** 250 μm , **(b)** 25 μm , **(c)** 5 μm **(f)** 0.6 μm **(i)** 0.8 μm .

Fig. 2. Increased frequency of spines with a small head in the *stratum radiatum* of APP/PS1 mice. **(a)** Representative projection images of dendrites from Tg- and APP/PS1 mice (63 \times , glycerol). **(b)** The spine density is similar in Tg- mice and in the plaque-free areas of APP/PS1 mice. **(c)** Spine density as a function of distance from apical trunk is similar in Tg- mice and APP/PS1 mice in plaque-free regions. **(d)** Constant average neck length for spines in APP/PS1 mice. **(e)** Cumulative frequency plots showing the distribution of spine neck length, indicating a similar distribution for both spine populations. **(f)** The frequency of small spines increases substantially in plaque-free areas

of APP/PS1 mice. **(g)** Cumulative frequency curves showing a shift towards smaller head volumes in APP/PS1 mice. **(h)** A bar graph depicting a significant increase in the frequency of small spines (volume < 0.03 μm^3) in the *stratum radiatum* of APP/PS1 mice. Scale bar, 0.6 μm .

Table 1. Plaque volume and density

Parameter	S. Oriens (N=4)	S. Radiatum (N=5)
Estimated total number of plaques	1551 ± 272.6	1985 ± 183.8
Plaque density (plaque/mm³)	1138 ± 214.4	1174 ± 113.0
Individual plaque volume (μm³)	0.019 ± 0.002	0.029 ± 0.003
Volume occupied by plaques (%)	1.421 ± 0.201	1.554 ± 0.195

Detailed Methods

Intracellular injections with Alexa 594

Mice were anesthetized with pentobarbital (0.04 mg/kg) and transcardially perfused with 20 ml phosphate buffer (PB) followed by 100 ml of 4% paraformaldehyde (pH 7.4) prepared in the same buffer. The brains were post-fixed in the same solution for 24 h, and coronal sections (150 μ m) were obtained on a vibratome and labelled with 10⁻⁵ M 4,6-diamidino-2-phenylindole (DAPI, Sigma D9542). Pyramidal neurons in CA1 were injected individually with Alexa594 (Invitrogen, Eugene, OR) by passing a steady hyperpolarizing current through the electrode (0.5 to -1.0 nA, Fig. 1 a-b). The current was applied until the distal tips of each neuron fluoresced brightly.

Morphology

Confocal microscopy. For each pyramidal neuron (5-7 neurons from each mouse, 6-7 mice per group), 1-5 randomly selected dendrites were scanned from the soma (basal dendrites) or apical trunk (apical dendrites) to the tip (125 dendrites total). In APP/PS1 mice, dendrites located within the plaques were also scanned. For each stack, the laser intensity and detector sensitivity were set so that the fluorescence signal from the spines occupied the full dynamic range of the detector. Therefore, while scanning, some pixels were saturated in the dendritic shaft but no pixels were saturated in the spines. In stacks containing images of A β plaques (green) the green channel was deleted. The stacks were coded and the codes were not broken until the quantitative analysis had been completed.

Spine density. Dendritic spine density was determined by tracing the image of the acquired dendrites in three dimensions (with NeuroLucida). Spines were marked during tracing and all protrusions were considered as spines, applying no correction factors to the spine counts. After tracing all the dendrites, each 2-channel stack (containing the green channel with amyloid plaques) was viewed with Imaris and we determined whether a dendrite entered a plaque (Knafo et al., 2009a). The traced dendrites were viewed with NeuroLucida and the corresponding stack with the green channel was opened. The traced dendrites were categorized as dendrites that passed through an amyloid plaque, or dendrites whose entire length was in a plaque-free area.

The reconstructed data were exported to NeuroLucida Explorer (MicroBrightField Inc., Williston, VT, USA) for quantitative analysis. Spine density was calculated for each dendrite by dividing the dendritic length by the number of spines. Spine density was also analyzed as a function of its distance from its origin (Sholl analysis), dividing the length of the dendritic segment by the number of spines in each 10 μm stretch from the origin.

Head volume measurement. Intensity thresholds were applied to each dendritic segment to generate a model of the data that was visualized as a solid surface (the Spot module, Imaris). With this module, volume based measurements are added to the volume rendering. The Spots module models point-like structures in the data (e.g., dendritic spines) providing a procedure to automatically detect such structures, an editor to manually correct any errors detected, a viewer to visualize the point-like structures as spheres, and a statistics output that includes the volume of the spine heads (supplemental figure 1 b). A solid surface that exactly matched the contours of the head was created for each dendritic spine (Fig. 1 i). The image of each dendrite was then rotated in three dimensions and examined to ensure that the solid surface created for each spine head was correct. Headless spines were extremely rare and they were not included in the analysis. Having taken the measurements, the 2-channels stacks were opened to view the plaques and the spines were categorized according to their location (within or outside of plaques). As described previously in an electron microscopy study of hippocampal dendritic spines (Trommald and Hulleberg, 1997), we did not observe a multimodal distribution for neck length or for head volume (Fig. 1-2). Consequently, we were unable to identify spine groups such as thin, stubby or mushroom (Harris et al., 1992). Therefore, we chose to describe spine morphology using measured dimensions rather than shape categories.

Neck length measurement. To measure the neck length, each dendrite was visualized with the Volume mode of Imaris. Individual spine necks were measured manually in three dimensions from the interface of the spine neck with the dendritic stalk to the beginning of the spine head (MeasurementPro module) while rotating the dendritic image (Knafo et al., 2009a). If the spine head was connected directly to the dendritic stalk, the neck length was recorded as zero. As the resolution in the z axis is significantly

lower than in the x-y axes, spines protruding perpendicular to the dendritic stalk in the z axis were not measured. Thus, approximately 60% of spines were measured.

Estimation of the volume and number of plaques

Immunocytochemistry. In slices taken from brains of the same mice used for the morphological studies, amyloid plaques were stained with an anti-human A β antibody in systematically sampled coronal sections (50 μ m thick, every sixth section in the hippocampus). A pilot study confirmed that this antibody exclusively marks thioflavin-s positive plaques (Knafo et al., 2009a). Free-floating sections were pretreated with 55% formic acid (Sigma-Aldrich, ACS) and washed with 0.1 M PB. Sections were treated with 1% H₂O₂ for 30 min to deplete the endogenous peroxidase activity, and they were then submerged for 1 h in PB with 0.25% Triton-X and 3% horse serum (Vector laboratories Inc., Burlingame, CA, USA). Sections were incubated overnight at 4°C with a mouse anti-human A β antibody (1:50; clone 6F/3D, Dako Glostrup, Denmark) and on the following day, the sections were rinsed and incubated for 2 h with a biotinylated horse anti-mouse antibody (1:200; BA-1000; Vector). The sections were then incubated for 1h in an avidin-biotin peroxidase complex (Vectastain ABC Elite PK6100, Vector) and finally, the staining was visualised with the chromogen 3, 3' diaminobenzidine tetrahydrochloride (DAB; Sigma-Aldrich, St Louis, MO, USA). After staining, sections were dehydrated, cleared with xylene and cover-slipped. As a control, some sections were processed as above but without the primary antibody, which produced no significant staining. Slices were then counterstained by the Nissl technique to visualize the hippocampal strata.

Unbiased stereology. Unbiased stereology was used to quantify and measure plaques since counting spherical plaques in two-dimensional cross sections provides an imprecise measure of the amount of A β (Stark et al., 2005). Using a stereotaxic atlas (Paxinos and Franklin, 2001) as a reference, eight slices at -1.1- -3.8 mm from bregma were analyzed in each brain. The Stereo Investigator software (Microbrightfield, Colchester, VT) was used to drive a motorized stage (Prior Scientific, Houston, Texas) on a dual optical head microscope (Olympus BX 51) and to mark and measure plaques at 40x (NA, 0.85) under brightfield optics. The software sequentially chose random counting

frames (100×100 µm) in the xyz axes, moving the motorized stage automatically within the previously delimited zones in the stratum oriens and the stratum radiatum.

To estimate the plaque volume after each amyloid plaque was marked, the edges the plaque were marked with the Nucleator probe (Moller et al., 1990). The number of labelled plaques was estimated using the optical fractionator method in Stereo Investigator. Plaques were marked only if their edges lay within the dissector area and they did not intersect forbidden lines, and if they came into the focus as the optical plane moved through the height of the dissector (20 µm). The guard zone thickness was set to 2 µm. The sum areas of the sampling site represented around 15% of the total area of the slice. This sampling method and the section interval was tested in a pilot experiment to ensure that the estimation of the number of plaques was representative of the total number.

Supplemental Figure 1.

Deconvolution and spine head volume determination.

- a. Representative projection of confocal images of CA1 dendrites before (left) and after deconvolution (right) Scale bar, 1 μm .
- b. The process of spine head volume quantification. Scale bar, 0.8 μm .
 - I. A dendritic segment after deconvolution.
 - II. Spots are used as seed points for a region to be grown as below.
 - III. The region around each seed point grows until a border stops its growth. The border is determined using local contrast as the experimental criterion that searches a perfect fit between the border and the spine head. Segmentation generates solid objects, some of which are spines while others are areas within the dendrites.
 - IV. The solid objects located in spine heads were selected the statistical analysis.

Supplemental Figure 2.

A photomicrograph depicting the hippocampus with amyloid plaques that were stained with an anti-human A β antibody and Nissl counterstained to identify the hippocampal strata. Scale bar, (a) 300 μm .

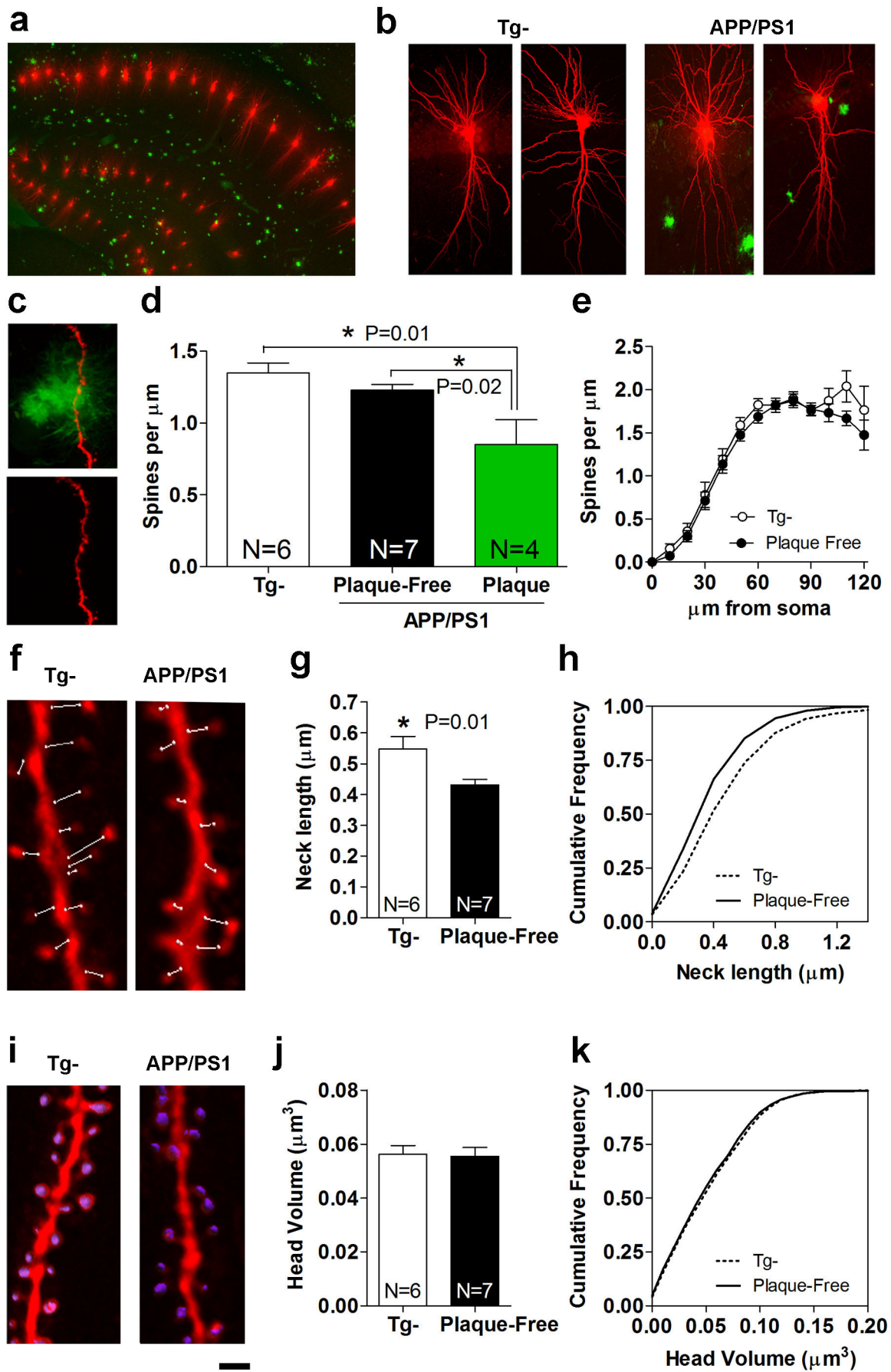


Figure 1

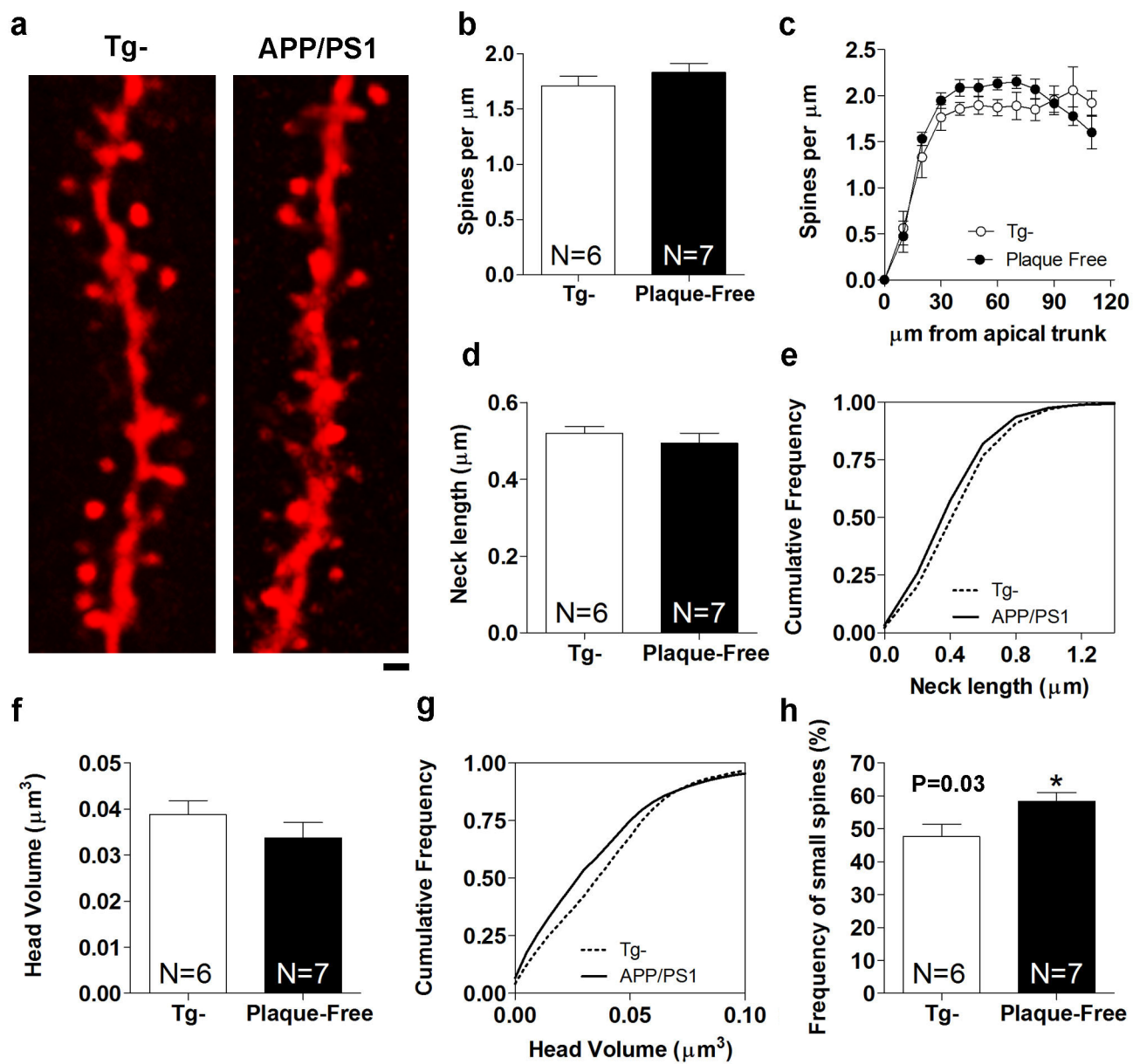
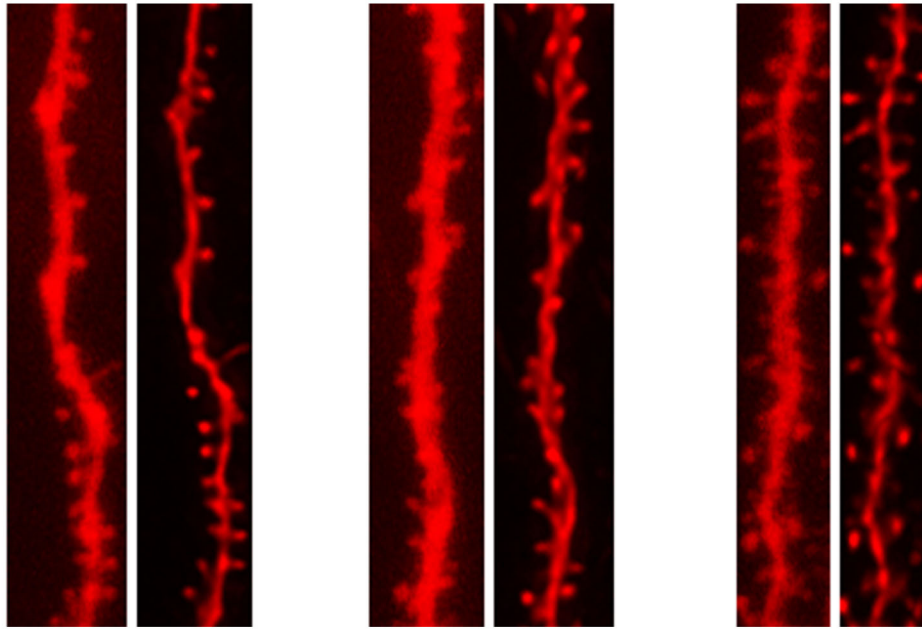
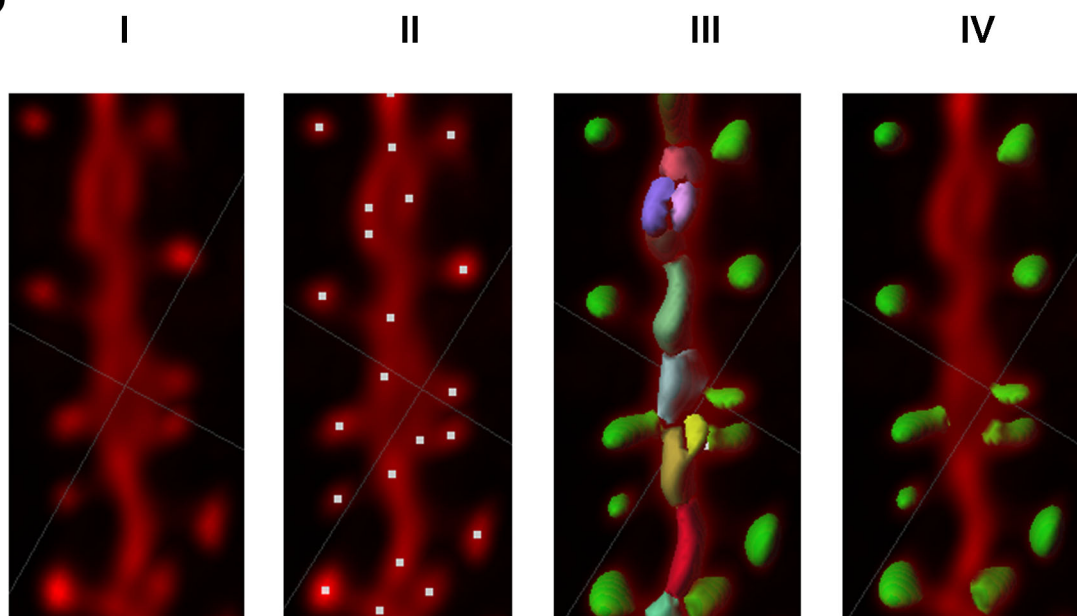


Figure 2

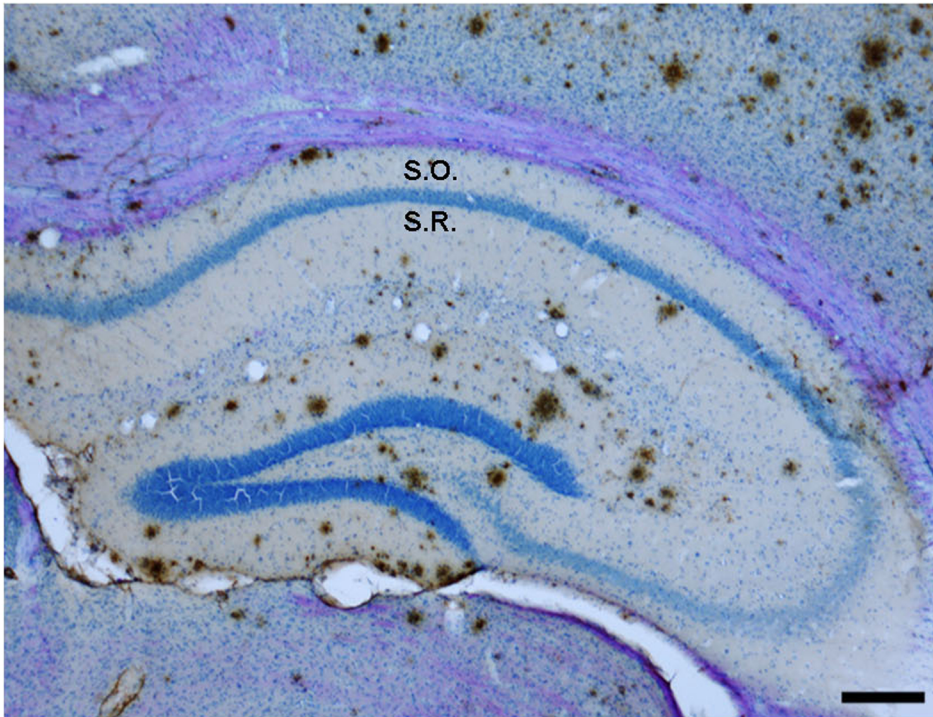
a



b



Supplemental figure 1



Supplemental figure 2